Lawrence Berkeley National Laboratory

Title
ELECTRONIC BAND STRUCTURE AND OPTICAL PROPERTIES OF PbTe, PbSe, AND PbS

Permalink
https://escholarship.org/uc/item/9b7149xf

Authors
Kohn, S.E.
Yu, P.Y.
Petroff, Y.
et al.

Publication Date
1972-08-01

RECEIVED
LAWRENCE
RADIATION LABORATORY

LIBRARY AND
DOCUMENTS SECTION

ELECTRONIC BAND STRUCTURE AND OPTICAL PROPERTIES OF PbTe, PbSe, AND PbS

S. E. Kohn, P. Y. Yu, Y. Petroff, Y. R. Shen,
Y. Tsang, and M. L. Cohen

August 1972

DISCLAIMER

0 0 0 0 0 8 0 0 9 3

UNIVERSITY OF CALIFORNIA

Lawrence Berkeley Laboratory
Berkeley, California

ELECTRONIC BAND STRUCTURE AND OPTICAL PROPERTIES OF PbTe, PbSe, AND PbS[†]

S. E. Kohn, P. Y. Yu,[‡] Y. Petroff,[*] Y. R. Shen, Y. Tsang, and M. L. Cohen

August 1972

Electronic Band Structure and Optical Properties of

PbTe, PbSe, and PbS[†]

S. E. Kohn, P. Y. Yu,[‡] Y. Petroff,[*] Y. R. Shen,

Y. Tsang, and M. L. Cohen

Department of Physics, University of California
and
Inorganic Materials Research Division,
Lawrence Berkeley Laboratory,
Berkeley, California 94720

ABSTRACT

By using the techniques of wavelength-modulation
spectroscopy, we have measured the reflectivity, $R(\omega)$, and the
derivative of the reflectivity, $1/R \, dR/d\omega$, for PbTe, PbSe, and
PbS from 1.5 to 6 eV. We have calculated the band structure,
frequency dependent dielectric function, density of states,
and derivative reflectivity spectrum for all three compounds
by the Empirical Pseudopotential Method.

I. INTRODUCTION

The narrow gap IV-VI semiconductors have been the object of extensive research over the past few years.[1-3] Compounds of Pb, Sn, and Ge have been studied, and a great deal is known about many of them. Particular emphasis has been placed on studies of the band edge properties and the fundamental gap. The location of the gap in the Brillouin zone,[4,5] the temperature and pressure dependence,[6,7] and the alloy dependence of the fundamental gap[7] have been studied extensively. Higher energy gaps have also been explored, but less is known about these gaps, and few experimental measurements have been made at higher energies.

In this paper we will present experimental optical data and theoretical band structure calculations for the lead chalcogenides PbTe, PbSe, and PbS. Several band structure calculations of these compounds are available in the literature using the APW method,[8-11] the Green's function method,[12] and two versions of the pseudopotential method.[4,13] All of these calculations have a minimum direct gap at the L point in the Brillouin Zone and many other features in common. There are differences, however, of the order of 1 eV for the energy bands away from the fundamental gap. These differences lead to different inter-pretations of the optical spectrum. These interpretations can be tested by calculating the optical constants in the visible and ultra-violet regions from the various band structure calculations, and then comparing the results with the measured optical spectra. Some calculations of this kind exist for the IV-VI semiconductors,[5,14,15] but not all of the above band structure calculations have been tested in this way.

Until recently, the only optical data in the visible and ultra-
violet spectral regions available for comparison to theoretical calcu-
lations have been the near-normal incidence reflectivity measurements
of Cardona and Greenaway,[16] and of Belle.[17] Since these experiments were
performed, derivative spectroscopic techniques have become very popular.
Aspnes and Cardona[18] have measured the electroreflectance of all three
lead salts. In their experiment, the electric field inside the samples
was considerably distorted from the ideal square wave shape because of
the high dielectric constant of the compounds. This made the usual
interpretation of the electroreflectance data more difficult.[18] Nishino,
et al.[19] have measured the electroreflectance and thermoreflectance of
PbSe, showing some differences between these measurements. We have
measured the wavelength-modulated reflectance of PbTe, PbSe, and PbS
from 1.5 to 6 eV at temperatures ranging from 5° to 300°K. The only
previously published wavelength-modulation reflectivity measurements
on any of these compounds is the work of Korn, Welkowsky, and Braunstein
on the $Pb_x Sn_{1-x} Te$ alloy system.[20]

We have also made Empirical Pseudopotential Method (EPM) calculations
of the band structure and $\varepsilon_2(\omega)$ spectrum of PbSe, and PbS. In addition,
by Kramers-Krönig transformations of the theoretical $\varepsilon_2(\omega)$ spectrum, the
reflectivity derivative spectrum $1/R \, dR/d\omega$ is calculated for PbTe, PbSe,
and PbS, and compared with the experimental measurements. These results
confirm the critical point assignment for the $\varepsilon_2(\omega)$ spectrum of PbTe
made previously by Cohen and Tsang.[7] By using the method of Gilat and
Dolling,[21] we have also calculated the density of states for all three
compounds.

II. EXPERIMENTAL PROCEDURE

The theory of wavelength-modulation spectroscopy and a description
of our experimental apparatus has been given elsewhere.[22] A double
beam optical system is used to normalize the reflectivity and to cancel
the background contributions to the derivative signal. The system is
operated in a configuration that measures $R(\lambda)$ and $dR/Rd\lambda$ simultaneously.
These results are then converted to $R(\omega)$ and $dR/Rd\omega$ by a relatively
simple computer manipulation.

Samples of all three compounds studied were bulk single crystals.
All of the samples used were cleaved to produce a clean, flat surface
and immediately placed in the optical dewar. The PbS crystal was large
and cleaved very well. The crystals of PbTe and PbSe were relatively
small, and their cleavages were not as perfect. Therefore, the absolute
magnitude of their relectivity measurements may not be correct, though
the relative measurements are still very acceptable. Once inside the
dewar, the samples were continuously maintained in a helium atmosphere.
Temperature control was achieved by flowing helium gas past the samples.
The spectra thus obtained are always reproducible.

III.   EXPERIMENTAL RESULTS

The experimentally measured reflectivity spectra $R(\omega)$, and derivative reflectivity spectra $dR/Rd\omega$ for PbTe, PbSe, and PbS are presented in Figs. 1, 2, and 3 along with theoretical calculations of the derivative spectra. All experimental results presented here were measured at 5°K. The main feature of the $dR/Rd\omega$ spectrum of PbTe agrees quite well with the results of Korn et al.[20] at 80°K. The derivative spectrum of all three compounds are strikingly similar. In all of the spectra, the E_2 and E_3 structures (in the notation of Cardona and Greenaway[16]) are well resolved. It is of particular interest to note the fine structure in the derivative spectra, particularly the existence of several peaks on the low energy side of the E_2 peak. These peaks are very similar in the spectra of all three compounds.

A Kramers-Kronig analysis of the $dR/Rd\omega$ spectra was performed to determine $\varepsilon_1(\omega)$, $\varepsilon_2(\omega)$, $d\varepsilon_1/d\omega$, and $d\varepsilon_2/d\omega$. The results of these calculations are presented in Figs. 4 and 5. A description of the method of calculation is given in the appendix. The results agree well with the calculations of Korn et al. in the case of PbTe. A quick glance at the $\varepsilon_2(\omega)$ and $d\varepsilon_2/d\omega$ spectra shows that the $d\varepsilon_2/d\omega$ spectra reveals considerably more structure than the $\varepsilon_2(\omega)$ spectra, and is therefore useful in identifying critical points and finer details of the optical spectrum.

Critical points obtained from the experimental spectra are listed in Table 1, along with experimental results of previous work. They were determined in two ways. First, critical points in the reflectivity were determined from the $dR/Rd\omega$ spectra. However, in the Kramers-Kronig

analysis of the experimental data, structures were shifted. Therefore,

a second list of critical point energies is given. These were determined

by comparing the theoretical $\varepsilon_2(\omega)$ with the $d\varepsilon_2/d\omega$ calculated from the

experimental data. The identification of the transitions then follows

the results of the theoretical calculation.

It is possible for structures in $1/R\ dR/d\omega$ to originate from

structures in $\varepsilon_1(\omega)$ rather than $\varepsilon_2(\omega)$. Aspnes and Cardona[18] showed

that, in electroreflectance, $\Delta R \propto -\Delta\varepsilon_1$ near the E_2 peak for all three

lead salts. A close comparison of our experimental data and the calcu-

lated $d\varepsilon_1/d\omega$ confirms this result.

IV. CALCULATION

The Empirical Pseudopotential Method (EPM) has now been widely

applied to many compounds, and the pseudopotential form factors for

many elements (extracted from different EPM band structure calculations)

are now available.[23] These existing pseudopotential form factors $V(q)$

for Pb, Se, and S are plotted respectively in Figs. 6, 7a, and 7b.[24]

A smooth curve is drawn through each set. The values of the form factors

can be read directly from these curves and can be properly scaled to

the lattice constants of PbSe and PbS to give the starting set of

form factors. The lattice constants of PbSe and PbS are taken to be

6.124 Å and 5.936 Å. Following the EPM scheme, these form factors are

slightly adjusted to fit several optical gaps. The choice of these

optical gaps are based on the assumption that the corresponding struc-

tures in the reflectivity spectrum in PbS and PbSe arise from the

same regions of the Brillouin zone as in PbTe, which have been analyzed previously.[4] In Table II are listed the starting set of form factors for PbS and PbSe interpolated and scaled from the Pb, S, and Se potentials,[23] as discussed above. This Table also contains the final set used in calculating the band structure and optical properties. The starting and final sets of form factors are remarkably close. The adjustment from the former to the latter set is minimal.

Spin-orbit coupling effects are included in the EPM calculation. The symmetric and antisymmetric spin orbit parameters λ_S, λ_A[23,25] in each material are chosen so that the ratio, λ_S/λ_A, corresponds to that of the constituent outer most core atomic spin orbit splitting.

The resultant band structure for PbSe and PbS are shown in Figs. 9 and 10 respectively. The minimum direct gap E_g is at the L point of the Brillouin zone with symmetry L_6^+ for the top valence band and symmetry L_6^- for the bottom conduction band, as in PbTe. The fundamental gaps are 0.172 eV and 0.287 eV respectively for PbSe and PbS. From studies of interband magneto-absorption, the corresponding experimentally measured values are 0.165 ± .005 eV and 0.286 ± 003 eV.[26] The overall features of the band structures for PbSe and PbS are similar and resemble that for PbTe (Fig. 8).

An intrinsic property of an EPM calculation is that the high energy bands crowd together as a result of the truncation of the Hamiltonian matrix.[23] This is illustrated by the PbS conduction bands at Γ. In a non-relativistic calculation, the conduction band symmetry at Γ for the lead salts would be Γ_{15}, $\Gamma_{25'}$, and Γ_{12}, counting upward in energy from the forbidden gap. The spin-orbit coupling splits the Γ_{15} into Γ_6^- and

Γ_8^-, $\Gamma_{25'}$ to Γ_7^+ and Γ_8^+ and Γ_{12} to Γ_8'. In PbS, the levels arising from $\Gamma_{25'}$ and Γ_{12} crowd together as they decrease in energy away from, and drop below, the Γ_8^- level of Γ_{15}. This same effect of the crowding of the higher energy bands is seen in the optical spectrum where the energies of the theoretical high energy structure (E_4, E_5, E_6) deviate somewhat from the measured data.

The imaginary part of the frequency dependent dielectric function $\epsilon_2(\omega)$ has the form

$$\epsilon_2(\omega) = \frac{e^2\hbar^2}{3\pi m^2\omega^2} \sum_{c,v} \int \delta(E_c(\underset{\sim}{k}) - E_v(\underset{\sim}{k}) - \hbar\omega)|\langle u_{\underset{\sim}{k},v}|\underset{\sim}{\nabla}|u_{\underset{\sim}{k},c}\rangle|^2 d^3\underset{\sim}{k} \qquad (1)$$

where $u_{\underset{\sim}{k},v}$ and $u_{\underset{\sim}{k},c}$ are the periodic parts of the valence and conduction band Bloch wavefunctions at $\underset{\sim}{k}$, $E_v(\underset{\sim}{k})$, and $E_c(\underset{\sim}{k})$ are the energies of these states. In the previous calculation of $\epsilon_2(\omega)$ for PbTe,[4] these wavefunctions and energies are obtained by diagonalizing a pseudopotential Hamiltonian at 356 mesh points in the irreducible part of the fcc cubic Brillouin zone. Approximately 3×10^6 random sampling points are then chosen using a Monte Carlo method. The energy eigenvalues and dipole matrix elements associated with each point are chosen by linear interpolation between the 356 mesh points. The prominent structure in the $\epsilon_2(\omega)$ originate from Van Hove singularities[23] at critical points where $\nabla_{\underset{\sim}{k}}(E_c(\underset{\sim}{k}) - E_v(\underset{\sim}{k})) = 0$. This can be more clearly seen if we write the k integration in Eq. (1) in terms of an integration over a surface S, corresponding to a constant interband energy difference $E_c(\underset{\sim}{k}) - E_v(\underset{\sim}{k})$. Assuming the dipole matrix to be a constant,

$$\epsilon_2 \sim \int \frac{dS}{\left| \nabla_k (E_c(\underset{\sim}{k}) - E_v(\underset{\sim}{k})) \right|} . \tag{2}$$

The expression on the right in Eq. (2) is the joint density of states .

Gilat and Dolling[21] developed a different method of calculation

first applied to a computation of the phonon density of states for a

cubic crystal.[27] This method proved to be of much higher resolution,

speed and accuracy in comparison with traditional random point sampling

methods. This method also involves dividing the irreducible section

of the first Brillouin zone into a cubic mesh, but instead of taking

discrete random points within the mesh, the constant frequency surfaces

inside every small cube are approximated by a set of parallel planes

(the directions of the planes are determined by $\nabla_k E(\underset{\sim}{k})$ at the mesh

points) and may be continuously integrated. Since the spectra contains

two important factors, the density of states and the transition probability

or dipole matrix element, these have to be known accurately when comparing

with high resolution experimentally measured spectra. Gilat et al.

obtain such accuracy for the density of states in references 21 and 27

by treating the matrix element of each cube as a constant. This implies

that fine details of the computed spectrum could be significantly

distorted. The computation of the matrix elements was later taken to

the same degree of accuracy as the density of states by Gilat and Kam.[23]

Along with the   experimental derivative reflectivity

data of the present work, we employ the Gilat scheme[21,27] in computing

the $\epsilon_2(\omega)$ for PbTe, PbSe and PbS. The pseudo-Hamiltonian is diagonalized

at 308 k points within the irreducible part of the Brillouin zone. The

mesh chosen is slightly different from the former calculation for

PbTe[4] in that here the mesh points are shifted away from symmetry

directions to avoid degeneracy, a necessary condition of the Gilat

Scheme. For this calculation, the dipole matrix element inside each

mesh is taken to be a constant equal to the value at the mesh point.

This is done for two reasons. First of all, previous experience with

PbTe indicates the usefulness of even the joint density of states in

determining the origin of the main structure in the reflectivity.

Secondly, a first order perturbation calculation on the dipole matrix

element at the mesh point to allow interpolation between points requires

far more computer time than doing a perturbation calculation on the

energy. Therefore, as a first attempt, we have taken the matrix elements

as constant in each small cubic mesh.

V. DISCUSSION

The final theoretical results are presented in Figs. 1 to 3 and

the theoretical dR/Rdω spectra are shown as dashed lines in Figs. 1-3,

together with the experimental spectra. The corresponding band struc-

tures for PbTe, PbSe, and PbS are given in Figs. 8-10 respectively.

In Fig. 11, the corresponding $\epsilon_2(\omega)$ spectra are shown. They agree

well with the $\epsilon_2(\omega)$ (Fig. 4) obtained from the experimental data.

The peaks in $\epsilon_2(\omega)$ are typically shifted down in energy from the

reflectivity spectrum by about 0.3 eV. The purpose of the theoretical

and experimental $\epsilon_2(\omega)$ curves (Figs. 11 and 4) are then to display the
position of the main peaks and shoulders, whereas the experimental and
theoretical derivative reflectivity spectra (Figs. 7, 9, and 11) are
designed to display the fine structure on the main ones. In Table 1
are listed our critical point assignments for PbTe,[7] PbSe and PbS using
the EPM calculations, and experimental values of critical points obtained
by us and by others[16,18] for the E_1-E_6 structures. Note that the
critical point assignment for all three materials are almost identical.
The values of E_4, E_5, and E_6 in the theoretical E_2 all group together
and are shifted down in energy, owing to the crowding of higher energy
conduction bands previously discussed.

To obtain the theoretical derivative spectrum, a Kramers-Krönig
transformation was performed on the theoretical $\epsilon_2(\omega)$ with an appropriate
tail function[29] for frequencies above ω_{cutoff}.[23] The respective
ω_{cutoff} for PbTe, PbSe, and PbS are 8.5 eV, 9.0 eV and 9.5 eV.

In the following discussion for the results of the PbTe, PbSe,
and PbS, the notations E_0-E_6 of Cardona and Greenaway[16] will be used
freely since the optical spectra for the three materials are indeed
qualitatively similar and discussion of a qualitative nature is applicable
to all three cases.

a) PbTe (Figs. 1 and 11a) - The solid curve in Fig. 11a is the
previous theoretical $\epsilon_2(\omega)$ calculation obtained from a random point-
sampling. The dotted curve is the present calculation using the Gilat
sampling scheme. Note how the critical points are accentuated in the
present (Gilat) scheme. The approximation that dipole matrix elements
are constant within each cube in the present scheme shows up most

obviously at the bumps at 0.3, 0.6, and 1.2 eV. The previous random point sampling scheme, which gives less resolution than the present scheme when structure arises from critical point singularities, does take account of the interpolation of dipole matrix elements within the cubic mesh and probably portrays more faithfully the actual $\epsilon_2(\omega)$. This is particularly true for the fine structure arising mainly from volume effects such as those at 0.3, 0.6, and 1.2 eV in PbTe. The theoretical $\epsilon_2(\omega)$ curve is therefore much sharper than the experimental $\epsilon_2(\omega)$ since the theoretical $\epsilon_2(\omega)$ expression contains the singularities as discussed above. The agreement for the energy positions and the general profile between the theoretically calculated and experimental $\epsilon_2(\omega)$ is good. The theoretical derivative reflectivity spectrum derived from $\epsilon_2(\omega)$ is extremely sensitive to any slight variation of the slope as well as the main peaks and shoulders in the $\epsilon_2(\omega)$. A comparison of the theoretical $1/R \, dR/d\omega$ with experiment in Fig. 7 is therefore encouraging. The theoretical $dR/Rd\omega$ would resemble the experimental curve at 3.35 eV if the E_3 shoulder in the theoretical $\epsilon_2(\omega)$ were slightly flatter. The experimental $dR/Rd\omega$ curve changes slope from negative to positive at 5.4 eV due to an upward turn of slope in $\epsilon_2(\omega)$ at energies just below the E_4 (6.3 eV as measured from reflectivity) structure. The theoretical E_4 value is at 7.1 eV, and thus the theoretical $dR/Rd\omega$ continues to have a negative slope at 5.4 eV. These results seem to indicate that our previous critical point assignment[4] for PbTe were essentially correct.

b) <u>PbSe</u> (Figs. 11b and 2) — One essential feature that differentiates PbSe from PbTe in the experimental $dR/Rd\omega$ spectrum (Figs. 2) is

the broad structure with small peaks between 2.0 and 3.1 eV in the

dR/Rdω spectrum. The corresponding structure in PbTe (Fig. 1) is

much narrower, having a width of only 0.5 eV. This can be understood

from the theoretical critical point analysis (Table 1) and the theoretical

$\epsilon_2(\omega)$ curves (Fig. 11a and 11b). For PbSe, there are critical points

at 1.9 eV, 2.3 eV, both with moderate dipole matrix elements. The main

peak E_2 is composed of two critical points with large dipole matrix

elements at 2.7 eV and 2.9 eV. This cluster of critical points with

increasing dipole matrix element gives rise to the gentle rising E_2

peak. In PbTe, the moderate dipole matrix elements of critical points

are at 1.07 and 1.27 eV while the large dipole matrix elements of

critical points are at 2.00 and 2.02 eV. Thus, the moderate matrix

elements in PbTe are farther away in energy from the large matrix

elements than in PbSe while the large matrix elements of PbTe occur

at almost the same energy. This results in a sharper and narrower E_2

peak in PbTe than in the case of PbSe.

The small structure on the main peaks arise from varying dipole

matrix elements for different regions of k space. As can be seen by

the above arguments, both the position of the critical points and the

dipole matrix elements are important to give the optical spectrum.

This point will be even more apparent when discussing PbS. The struc-

ture near the 4.4 eV region in the experimental dR/Rdω (Fig. 2) is

again due to the E_3 shoulder in $\epsilon_2(\omega)$ and the rise in slope at 6.1 eV

again arises because of the E_4 structure at 7.1 eV.

c) <u>PbS</u> (Figs. 11c and 3) -- The theoretical $\epsilon_2(\omega)$ in Fig. 11c

shows that in addition to the E_1-E_6 structure, there is an extra bump

between 3.5 and 4.1 eV. No critical point is found in this energy
region. A close examination of all the energy gaps that may contribute
to $\epsilon_2(\omega)$ in this energy range uncovers the following: 1) the contribu-
tion to this part of $\epsilon_2(\omega)$ arises from the same band transitions
essentially in neighboring cubic mesh, i.e., volume effect, (each
mesh covers an energy level of about 0.2 - 0.3 eV) and 2) the dipole
matrix elements of these neighboring mesh points vary by a factor of
two or three. Recall that the matrix element in each cubic mesh is
taken to be constant and equal to the value at the mesh point, whereas
the energy is allowed to vary continuously within the mesh. Therefore
in the continuous energy range of above 6.6 eV, the dipole matrix
element jumps discontinuously by about a factor of 2 to 3 at every 0.2
or 0.3 eV interval.

If one now uses linear interpolation for the matrix elements in
the continuous energy range of these particular neighboring cubic mesh
points in question, the resultant $\epsilon_2(\omega)$ between 3.5 eV and 4.1 eV will
follow the dotted line in Fig. 11c. In the region of the spurious
bump, there remains now only some smooth structure, which does show up
when transformed to the theoretical 1/R dR/dω in Fig. 3. This structure
deviates considerably in shape from the experiment 1/R dR/dω in the
region from 3.5 to 4.5 eV. The Gilat Scheme[21] would be necessary if
one were interested in obtaining an undistorted spectrum and retaining
the qualitative features of the fine structures of the optical spectrum,
because it takes into account the interpolation of the matrix elements
within each cubic mesh. The distortion of the fine structure is
especially important when the structure arises from volume effects. In

PbSe and PbTe, the E_3 critical points are close in energy to the E_2

critical points. The singularities help to mask the distortion of

fine structures arising from the approximation imposed on the dipole

matrix elements. We are less fortunate in PbS in that E_3 critical

points are much higher in energy than the E_2 critical points, allowing

volume effects to dominate in between. The structure between 2 - 3.5 eV

in the experimental $1/R \, dR/d\omega$ (Fig. 3) is even broader than the corres-

ponding one in PbSe. This is again a result of the clustering of

critical points at 1.6 eV, 1.9 eV, 2.94 eV, and 3.5 eV. Note the two

large matrix element critical points that give rise to the E_2 peak

(2.94 eV and 3.5 eV) are separate by 0.56 eV. This gives rise to a

very broad E_2 peak.

In measuring the reflectivity spectrum of PbS as a function of

temperature, we observed a pronounced sharpening in the fine structure

at 5.08 eV as the temperature decreases. This sharpening is observable

even between liquid nitrogen and liquid helium temperatures. This is

shown in Fig. 12. No other structure in the spectra of all three

compounds has a similar behavior. The sample used in this measurement

was n-type with a carrier concentration of $\sim 10^{16}/cm^3$ as obtained from

Hall effect measurements. However, when we repeated the measurement

on an n-type sample with a carrier concentration of $\sim 10^{18}/cm^3$, this

5.08 eV structure became less pronounced at low temperature, and did

not show appreciable change as the temperature varied from 80 to 5°K.

This result, similar to what was observed for the E_1 peaks of Ge,[30]

indicates that this structure is not simply due to band transitions.

The strong temperature dependence together with the dependence on the

carrier density seems to suggest that the structure may be due to excitonic effect. According to Herman et al.[11] the E_3 peak is due to M_1 and M_2 critical point transitions at Σ and Δ, and hence, based on the Toyozawa model,[31] hyperbolic excitons can exist in the E_3 peak. One may use the high dielectric constant of PbS to argue against the idea of excitons in PbS. However, in our case, the excitons involving electrons in the high conduction bands may see a smaller effective dielectric constant than even the high-frequency dielectric constant ϵ_∞. The free carriers tend to screen the attractive interaction between electrons and holes, and this would explain why the excitonic effect decreases with higher carrier concentration in our observation.

For completeness, we also present theoretical calculations of the density of states of PbTe, PbSe, and PbS in Fig. 13. Again, these are based on the EPM band structures and the Gilat sampling scheme. The valence band edge is taken to be the zero energy reference. The energy ranges from -12 to +12 eV. This energy range covers four valence bands and five conduction bands. The lowest valence band in the EPM calculation for the three materials are more than 13 eV below the top valence band edge. Since these band structures have given reasonable results in explaining the reflectivity data, one would anticipate that the density of states could also be useful in studying photoemission experiments.[32]

Wavelength-modulation spectroscopy has proved capable of detecting many fine structures in the optical spectrum of PbTe, PbSe, and PbS. The agreement of the experimental and theoretical $1/R \ dR/d\omega$ and $\epsilon_2(\omega)$ is quite good. Based upon these results, we conclude that the EPM gives

band structures of the lead chalcogenides that are essentially correct
throughout the Brillouin zone. With these band structures, we have
gained confidence in a more thorough understanding of the optical
properties of the lead chalcogenides. The computational techniques
may be improved by changing the approximation used in handling the
dipole matrix elements. If this is done, we believe that the band
structure calculations are capable of giving not only the main structure
but also the very fine structure in the optical reflectivity spectra.

APPENDIX

Kramers-Krönig Analysis

To obtain $\epsilon_1(\omega)$ and $\epsilon_2(\omega)$, we need to know both the absolute reflectivity, $R(\omega)$, and the corresponding phase angle, $\theta(\omega)$.[33] These two quantities are related by the Kramers-Krönig relation

$$\theta(\omega) = -\frac{\lambda}{\pi} \int_0^\infty d\lambda' \frac{\ln R(\lambda')}{(\lambda')^2 - \lambda^2}. \tag{3}$$

This can be transformed into the form

$$\theta(\lambda) = -\frac{1}{2\pi} \int_0^\infty d\lambda' \frac{d\ln R}{d\lambda}(\lambda') \ln\left|\frac{\lambda+\lambda'}{\lambda-\lambda'}\right| \tag{4}$$

which is more appropriate for our own case, since we measure $d\ln R/d\lambda$ with greater accuracy than R. This method of calculation has the disadvantage that the function $\ln|\lambda+\lambda'/\lambda-\lambda'|$ does not go to zero as fast as $1/(\lambda'^2-\lambda^2)$ as λ' becomes very different from λ. Hence, the calculation is a little more sensitive to the extrapolation conditions used for the low and high energy limits of the integral.

By differentiating Eq. (4) with respect to λ, we have

$$\frac{d\theta}{d\lambda}(\lambda) = -\frac{1}{\pi} \int_0^\infty d\lambda' \frac{d\ln R}{d\lambda}(\lambda') \frac{\ln R(\lambda')}{(\lambda')^2 - \lambda^2}. \tag{5}$$

The derivatives of ϵ_1 and ϵ_2 can be then calculated from $d\ln R/d\lambda$ and $d\theta/d\lambda$.

In evaluating the integrals for θ and $d\theta/d\lambda$, it is necessary to make truncating approximations for the low and high energy limits of

the integrals. It is well known that the reflectivity of semiconductors

becomes approximately constant at very low energies. It is common to

take $R(\lambda)$ as constant for long wavelengths when computing θ via Eq. (3).[33]

We have made a similar approximation $d\ell nR/d\omega = 0$ for long wavelengths.

Also, structure in $d\ell nR/d\lambda$ far away from the long wavelength limit of

Eqs. (4) and (5) tend to oscillate around zero, giving small contributions

to the integrals. At very high energies, it is expected, from a Drude

type of dielectric function, that the reflectivity should decrease

roughly as ω^{-4}. Therefore, we approximated a functional dependence for

R of ω^{-A}, where A is an adjustable parameter around 4. To make the

calculations less sensitive to A, the room temperature reflectivity

data of Cardona and Greenaway[16] from 6 to 20 eV were used in computing the

integrals. The results are very insensitive to the choice of A used.

Varying A by over a factor of 2 does not change the shape of the curves

appreciably, but does change the overall magnitudes somewhat. The

absolute magnitudes of the curves are also somewhat in error because

the absolute magnitude of $1/R \, dR/d\lambda$ is a little uncertain, although this

does not have a very strong effect in the Kramers-Kronig analysis.

References

†   Supported in part by the U. S. Atomic Energy Commission and the

     National Science Foundation, Grant GP

‡   IBM Postdoctoral Fellow.

*   On leave from the University of Paris.

1.   "International Colloquium on IV-VI Compounds, Gif-sur-Yvette, France,
     15-18 July 1968", J. Phys. (Paris) Suppl. 29, C4 (1968).

2.   "The Physics of Semimetals and Narrow Gap Semiconductors: Proceedings
     of the Conference held at Dallas, Texas, 20-21 March 1970",
     D. L. Carter and R. T. Bates, eds., (Pergamon, New York, 1971).

3.   "Proceedings of the Conference on the Physics of IV-VI Compounds
     and Alloys, Philadelphia, 1972", (to be published in J. of Non-
     Metals).

4.   Y. W. Tung and M. L. Cohen, Phys. Rev. 180, 823 (1969); errata
     Phys. Rev. B2, 1216 (1970); Y. W. Tung and M. L. Cohen, Phys Letters
     29A, 236 (1969).

5.   Y. W. Tsang and M. L. Cohen, Solid State Comm. 9, 261 (1971).

6.   Y. W. Tsang and M. L. Cohen, Phys. Rev. B3, 1254 (1971).

7.   M. L. Cohen and Y. W. Tsang, ref. 2, p. 303.

8.   L. E. Johnson, J. B. Conklin, Jr., and G. W. Pratt, Jr., Phys.
     Rev. Letters 11, 538 (1963); J. B. Conklin, Jr., L. E. Johnson,
     and G. W. Pratt, Jr., Phys. Rev. 137, A1282 (1965).

9.   L. G. Ferreira, Phys. Rev. 137, A1601 (1965).

10. H. Overhof and U. Rössler, Phys. Stat. Solidi 37, 691 (1970).

11. S. Rabii, Phys. Rev. 167, 801 (1968); S. Rabii, Phys. Rev. 173,
     918 (1968).

12. F. Herman, R. L. Kortum, I. Ortenburger, and J. P. Van Dyke, J. Phys. (Paris) Suppl. $\underline{29}$, C4-62 (1968).

13. P. J. Lin and L. Kleinman, Phys. Rev. $\underline{142}$, 478 (1966).

14. M. L. Cohen, Y. Tung, and P. B. Allen, J. Phys. (Paris) $\underline{29}$, C4-163 (1968).

15. D. D. Buss and N. J. Parada, Phys. Rev. B$\underline{1}$, 2692 (1970).

16. M. Cardona and D. L. Greenaway, Phys. Rev. $\underline{133}$, A1685 (1964).

17. M. L. Belle, Soviet Phys.-Solid State $\underline{5}$, 2401 (1964) and $\underline{7}$, 480 (1964).

18. D. E. Aspnes and M. Cardona, Phys. Rev. $\underline{173}$, 714 (1968).

19. T. Nishino, H. Ogawa, and Y. Hamaka, J. of Phys. Soc. of Japan $\underline{30}$, 1113 (1971).

20. D. M. Korn, M. Welkowsky, and R. Braunstein, Solid State Comm. $\underline{9}$, 2001 (1971); D. M. Korn and R. Braunstein, Phys. Rev. B$\underline{5}$, 4837 (1972).

21. G. Gilat and G. Dolling, Phys. Letters $\underline{8}$, 304 (1964).

22. R. R. L. Zucca, Ph.D. Thesis, University of California, Berkeley, 1970.

23. M. L. Cohen and V. Heine, Solid State Physics $\underline{24}$, H. Ehrenreich, F. Seitz, and D. Turnbull, eds., (Academic Press, New York, 1970).

24. The data points in Fig. 6, 7a, and 7b are taken directly from Reference 22, Tables 15, 16, page 212 and 215.

25. Y. W. Tsang, Ph.D. Thesis, University of California, Berkeley, 1970.

26. D. L. Mitchell, E. D. Palik, and J. N. Zemel, Physics of Semiconductors, Paris (1964), Mittulin, editor (Academic Press, 1964), p. 325.

27. G. Gilat and L. J. Rankenheimer, Phys. Rev. 144, 390 (1966).

28. G. Gilat and Z. Kam, Phys. Rev. Letters 22, 715 (1969).

29. J. P. Walters and M. L. Cohen, Phys. Rev. 183, 763 (1969).

30. Y. Petroff, S. E. Kohn, and Y. R. Shen, First International
     Conference on Modulation Spectroscopy, Tucson, Arizona, November
     1972.

31. Y. Toyozawa,   M. Inoue, M. Okazaki, and E. Hanamura J. Phys. Soc.
     Japan, Suppl. 21, 133 (1967).

32. A very good agreement with the theoretical valence band density
     of states has been obtained by preliminary photoemission measure-
     ments on PbTe. R. Pinchaux, Y. Petroff, D. Dagneaux and
     M. Balkanski, Conference on Physics of IV-VI Compounds and Alloys,
     Philadelphia, 24-25 March 1972.

33. M. Cardona, Optical Properties of Solids, Nudelman and Mitra, eds.
     (Plenum, New York, 1969), p. 137.

Table Captions

Table I. Critical point energies of a) PbTe, b) PbSe, and c) PbS. The

second column contains critical points derived from experimentally

measured $1/R\ dR/d\omega$. The third column has critical points from the

$d\varepsilon_2/d\omega$ spectra obtained by Kramers-Krönig analysis. The fourth

column contains the results of EPM calculations.

+   Reference 4

(a)   Reference 16

(b)   Reference 18

(w)   Weak

*   Structure in $1/R\ dR/d\omega$ due to structure in ε_1.

Table II. The interpolated and final set of pseudopotential form factors

used for the calculation of the band structures of PbSe and PbS.

TABLE 1A

PbTe

Region	Other Experimental Data	1/R dR/dω	dε$_2$/dω	Theory	CP Symm.	Transition
E$_o$	.19(a)			.19	M$_o$	L(5 → 6)
E$_1$	1.24			1.07	M$_1$	Σ(5 → 7)
				1.27	M$_o^1$	L(5 → 7)
E$_2$	2.18(b)	2.16(w)*	2.1	2.00	M$_1$	Σ(5 → 7)
		2.25*	2.2	2.03	M$_2^1$	Δ(5 → 6)
	2.45(b)	2.36*	2.3			
		2.56(w)*				
E$_3$	3.5(a)	3.47	3.3	2.78	M$_2$	Δ(4 → 6)
		4.83(w)	4.9	3.1	M$_1^2$	Σ(4 → 7)
		5.9	5.9			
E$_4$	6.3(a)					
E$_5$	7.8(a)					Volume effects Transitions near X
E$_6$	11.2(a)					

TABLE 1B

PbSe

Region	Other Experimental Data	$1/R\, dR/d\omega$	$d\varepsilon_2/d\omega$	Theory	CP Symm.	Transition
E_0	.165(c)			.172	M_0	$L(5 \to 6)$
E_1	1.59(a)			1.6	M_0	$L(5 \to 7)$
	1.54(b)	1.97(w)⎱	2.0 ⎱	1.9	M_1^0	$\Sigma(5 \to 6)$
	1.78(b)	2.18(w)⎰	2.15⎰	2.3	M_0^1	$L(4 \to 6)$
E_2	2.95(a)	2.84(w)*⎱	2.65⎱	2.7	M_1	$\Sigma(5 \to 7)$
	3.12(a)	3.12* ⎰	2.8 ⎰	2.9	M_2^1	$\Delta(5 \to 6)$
	3.3(b)					
	3.8(b)					
E_3	4.5(a)	4.47 ⎱	4.40⎱	4.2	M_2	$\Delta(4 \to 6)$
	4.6(b)	5.52 ⎰	5.3 ⎰	4.3	M_1^2	$\Sigma(4 \to 7)$
E_4	7.1(a)					
E_5	9.1(a)					
E_6	12.5(a)					

Volume effects
Transitions near Γ and X.

PbS

Region	Other Experimental Data	$1/R\ dR/d\omega$	$d\epsilon_2/d\omega$	Theory	CP Symm.	Transition
E_0	.286			.287	M_0	$L(5 \to 6)$
E_1				1.6	M_0	$L(5 \to 7)$
	1.85(a),(b)	1.9	2.0	1.9	M_1	$\Sigma(5 \to 6)$
	1.98(b)	2.15	2.1			
		2.46	2.3			
		2.85	2.5			
E_2	3.49(a)	3.35*	3.0			
	3.7(b)	3.66*	3.3	2.94	M_1	$\Sigma(5 \to 7)$
	4.0(b)	4.01*	3.9(w)	3.5	M_2^1	$\Delta(5 \to 6)$
	4.6(b)	4.5*				
E_3		5.08	5.0	4.92	M_1	$\Sigma(4 \to 7)$
	5.27(a)	5.31	5.2	5.1	M_2^1	$\Delta(4 \to 6)$
		5.75(w)				
E_4	8.1(a)					
E_5	9.8(a)			Volume effect Transitions near Γ and X.		
E_6	13.9(a)					

TABLE 2

	PbSe		PbS	
	Interpolated	Final Adjusted	Interpolated	Final Adjusted
$V^S(4)$	$-.2334$ Ry	$-.2377$ Ry	$-.256$ Ry	$-.2532$ Ry
$V^S(8)$	$-.0171$	$-.0171$	$-.0116$	$-.0181$
$V^S(12)$	$.0097$	$.0097$	$.0242$	$.0242$
$V^A(3)$	$.0657$	$.0735$	$.091$	$.0859$
$V^A(11)$	$.0154$	$.01224$	$.0154$	$.01038$

FIGURE CAPTIONS

Fig. 1. Reflectivity and derivative reflectivity of PbTe at 5°K. The

dotted curve is the theoretical 1/R dR/dω spectra calculated by

the EPM.

Fig. 2. Reflectivity and derivative reflectivity of PbSe at 5°K. The

dotted curve is the theoretical 1/R dR/dω spectra calculated by

EPM.

Fig. 3. Reflectivity and derivative reflectivity of PbS at 5°K. The

dotted curve is the theoretical 1/R dR/dω spectra calculated by

EPM.

Fig. 4. $\varepsilon_1(\omega)$ and $\varepsilon_2(\omega)$ of a) PbTe, b) PbSe, and c) PbS calculated

by Kramers-Krönig analysis of the 1/R dR/dω spectra.

Fig. 5. $d\varepsilon_1/d\omega$ and $d\varepsilon_2/d\omega$ of a) PbTe, B) PbSe, and c) PbS calculated

by Kramers-Krönig analysis of the 1/R dR/dω spectra.

Fig. 6. Pseudopotential form factors for Pb. The points are derived

from PbTe data.[23,24]

Fig. 7. Pseudopotential form factors for a) Se and b) S.[23,24]

Fig. 8. Energy band structure of PbTe (a reproduction from Ref. 4).

Fig. 9. Energy band structure of PbSe.

Fig. 10. Energy band structure for PbS.

Fig. 11. The theoretical imaginary part of the frequency dependent

dielectric function $\varepsilon_2(\omega)$ for a) PbTe, b) PbSe, and c) PbS.

Fig. 12. Temperature dependence of the derivative reflectivity, 1/R dR/dω,

of PbS around the E_3 structure.

Fig. 13. Density of states (number of states per eV per primitive cell)

for a) PbTe, b) PbSe, and c) PbS.
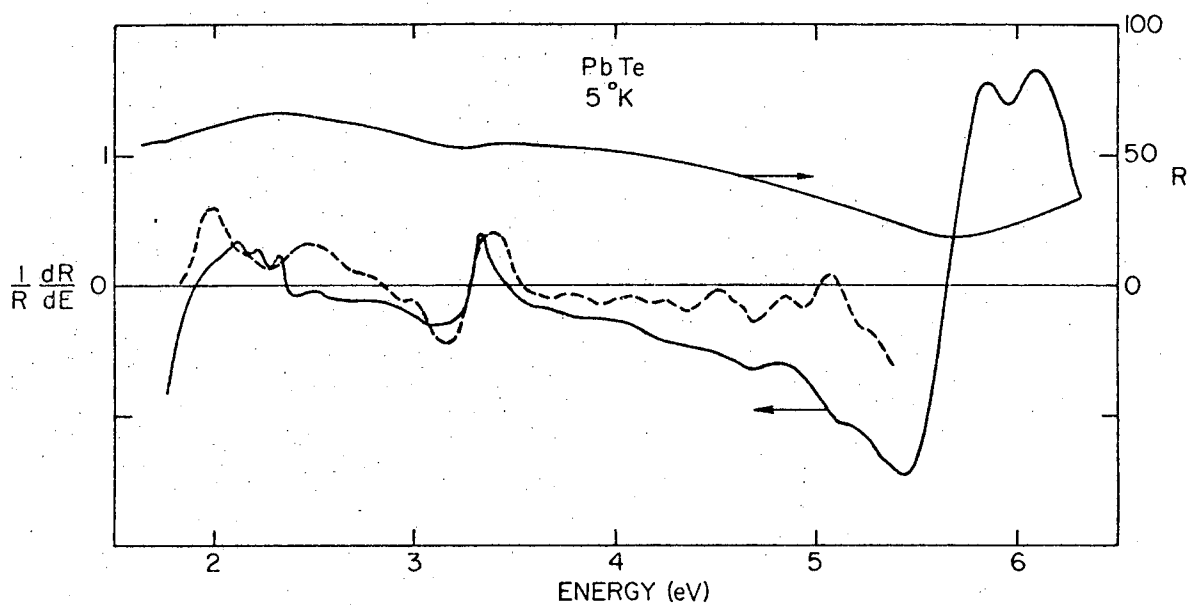
XBL 723-6082

Fig. 1
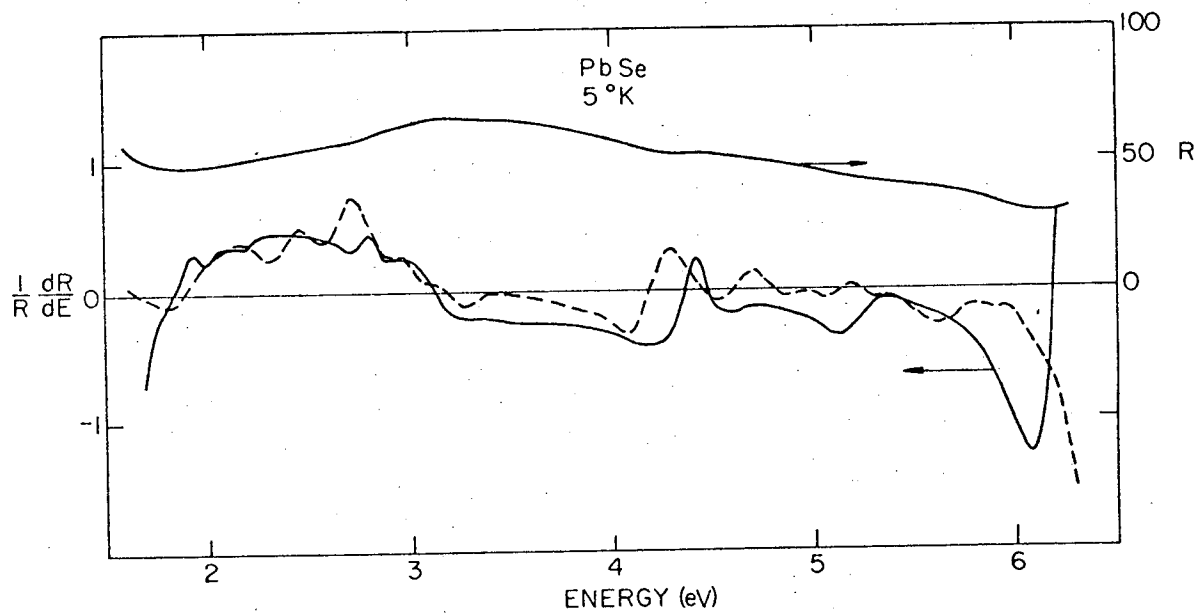
XBL 723-6079

Fig. 2

LBL-1132
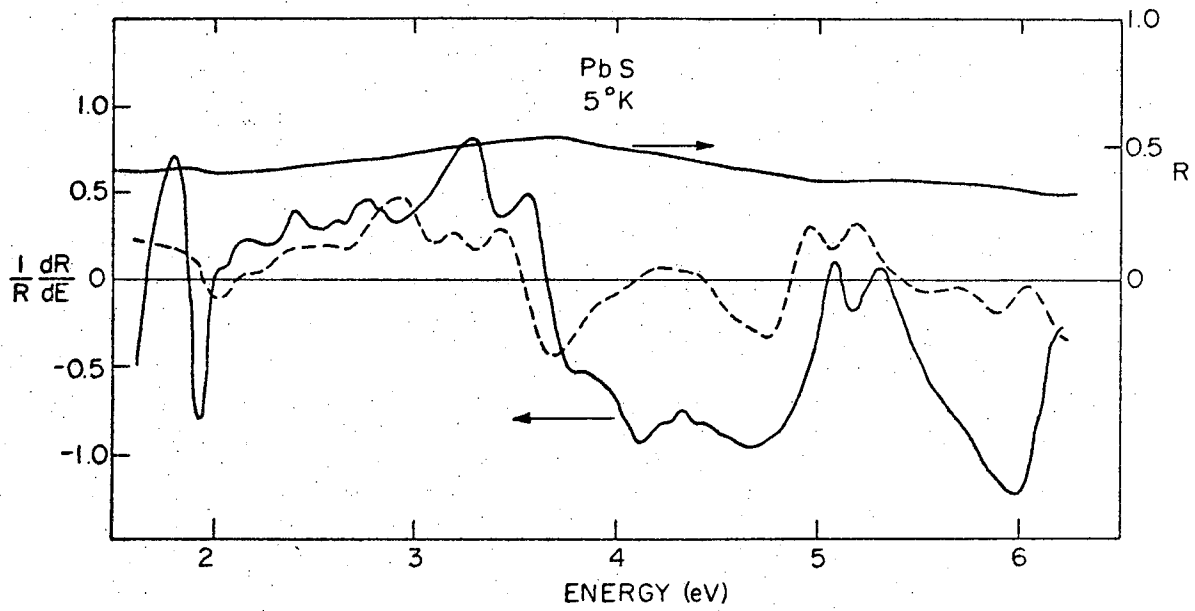
XBL 726- 6469

Fig.   3

(a)

(b)

(c)

Fig. 4

(a)

XBL 723-6084

(b)

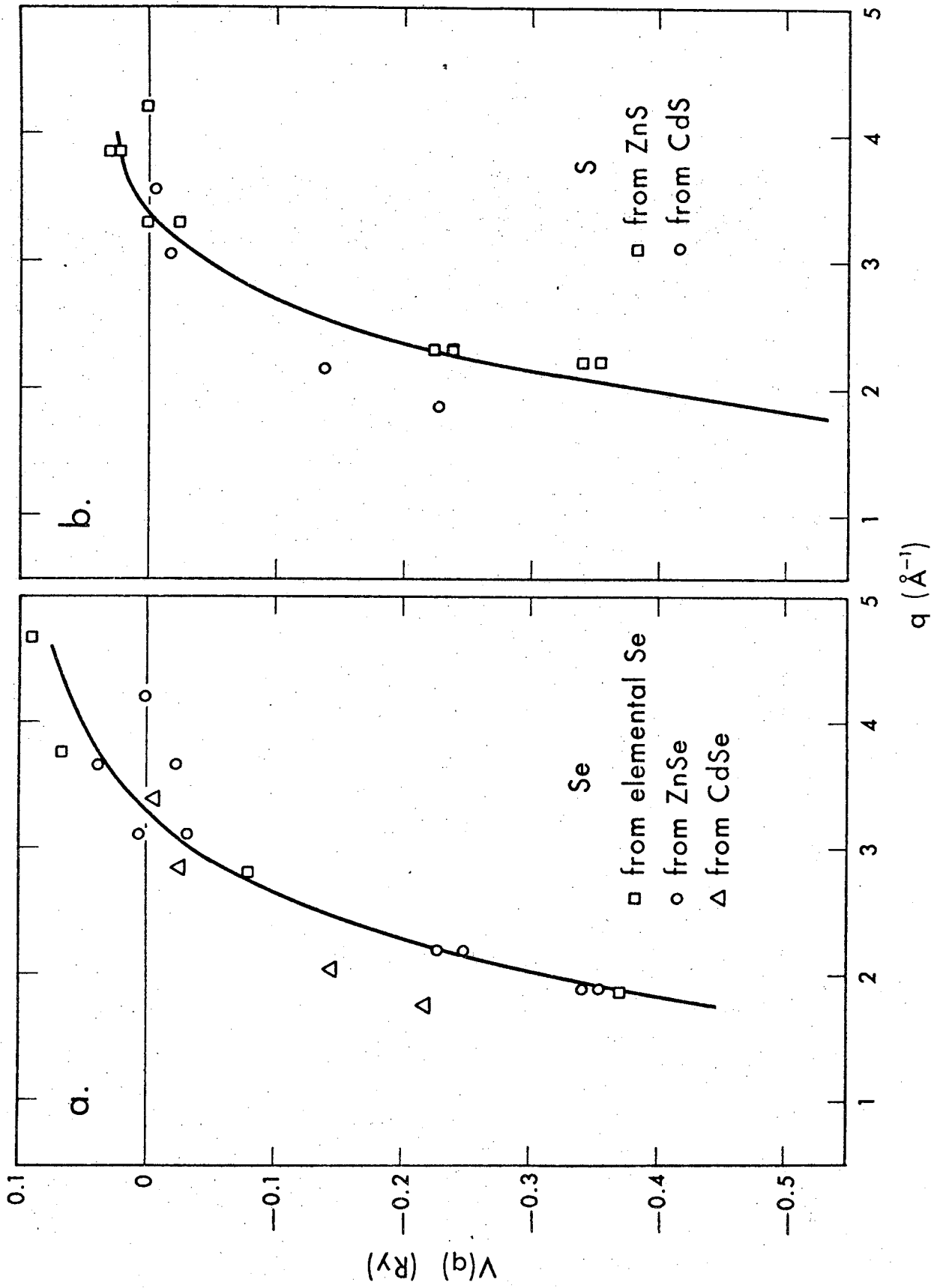XBL 723-6083
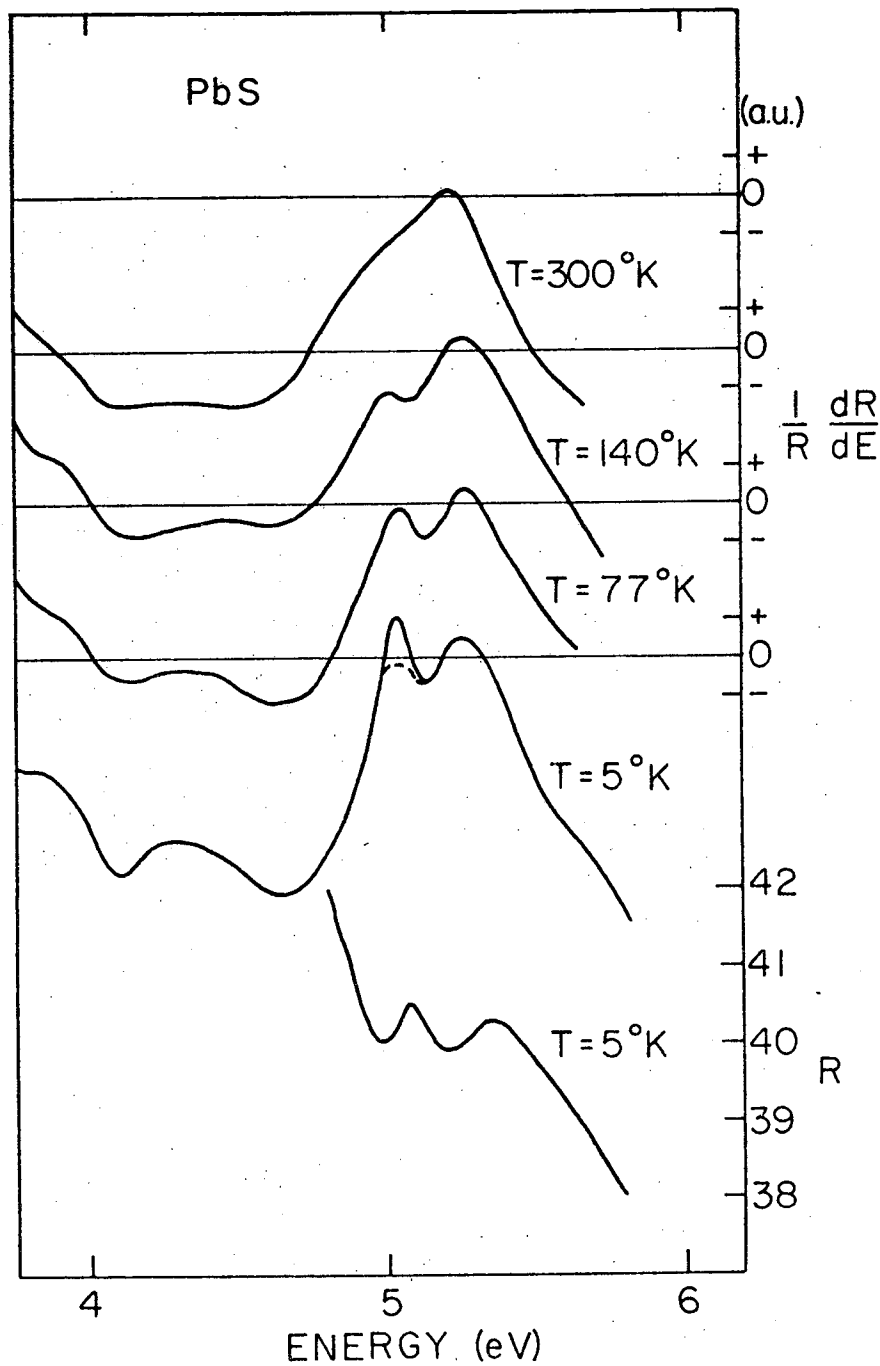
(c)
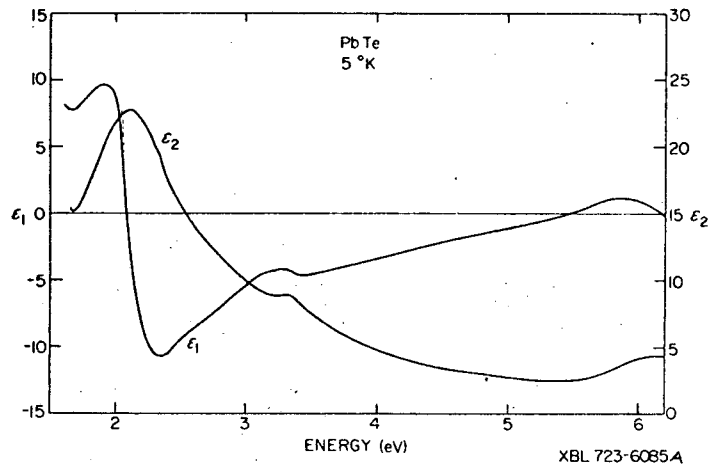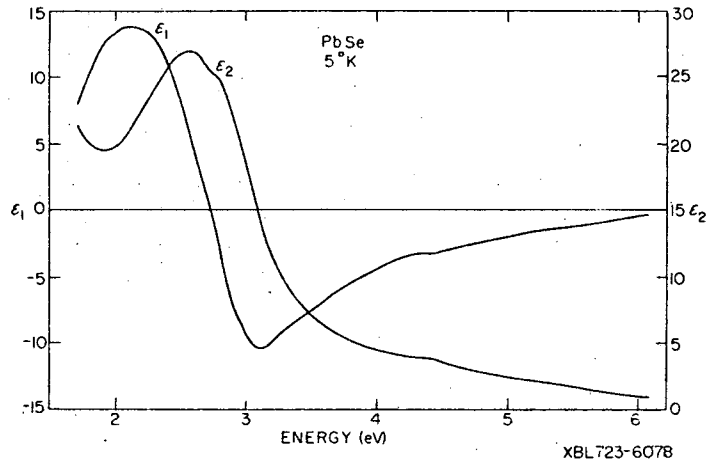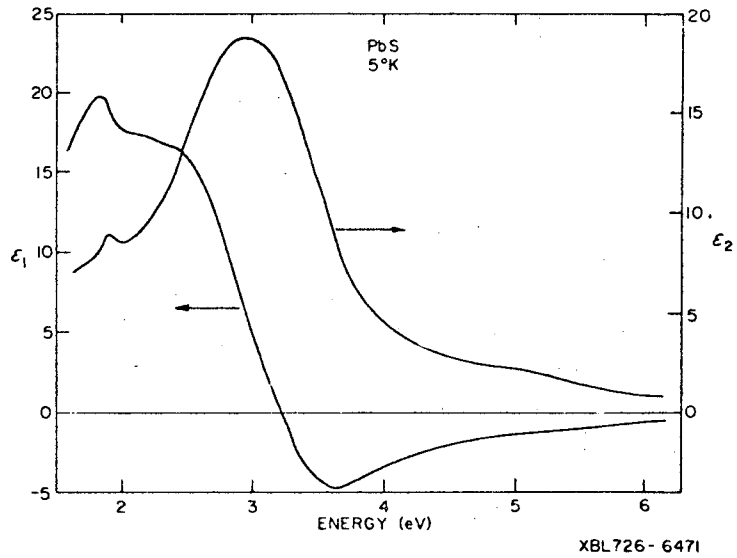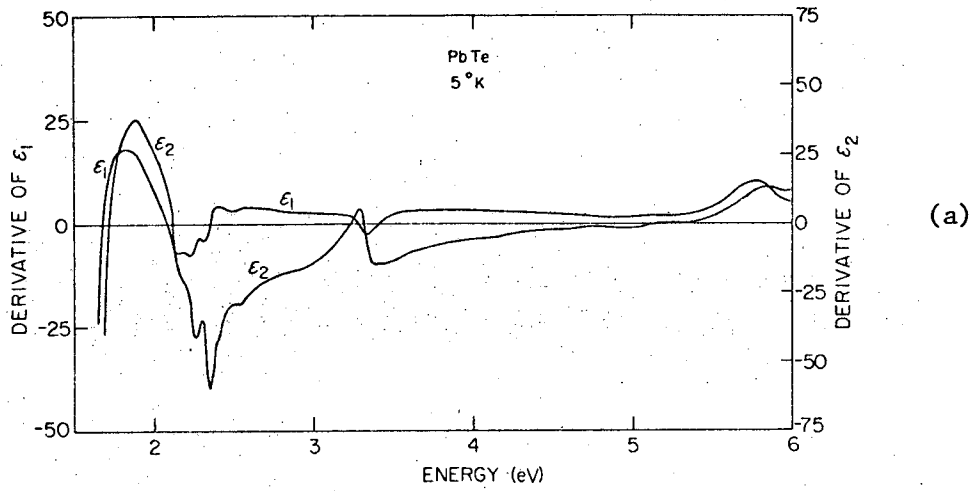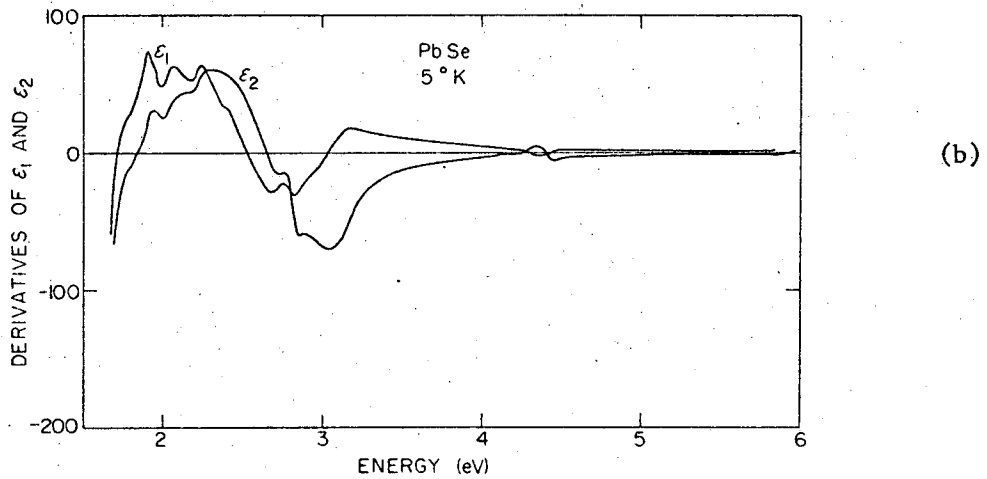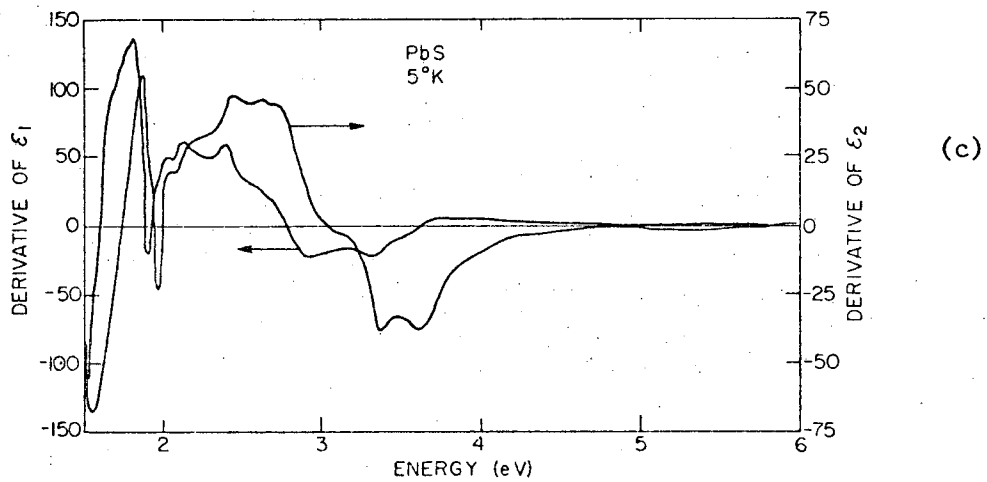
XBL 726-6470

Fig. 5

Fig. 6

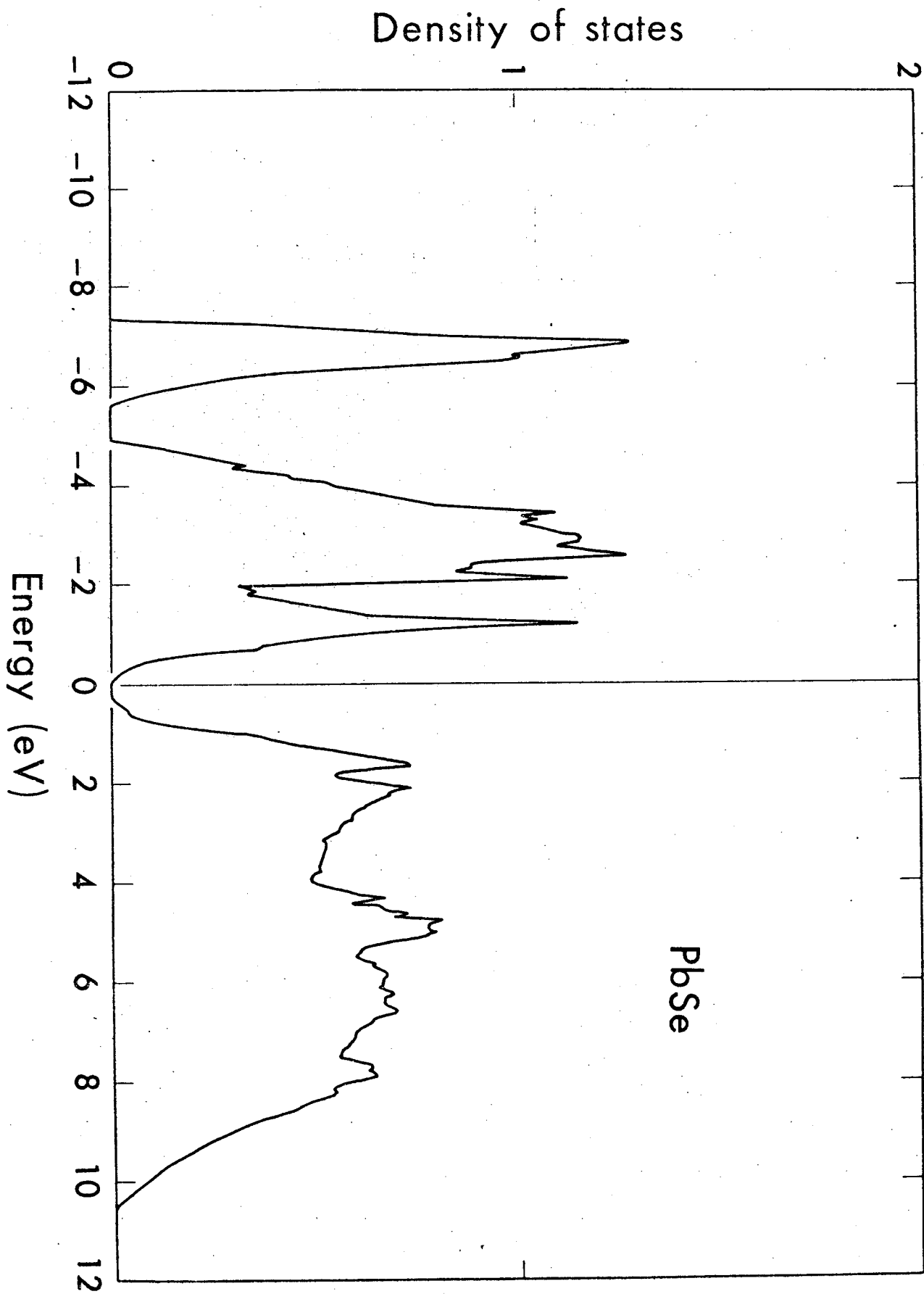Fig. 7

Fig. 8

Fig. 9

PbS

Fig. 10
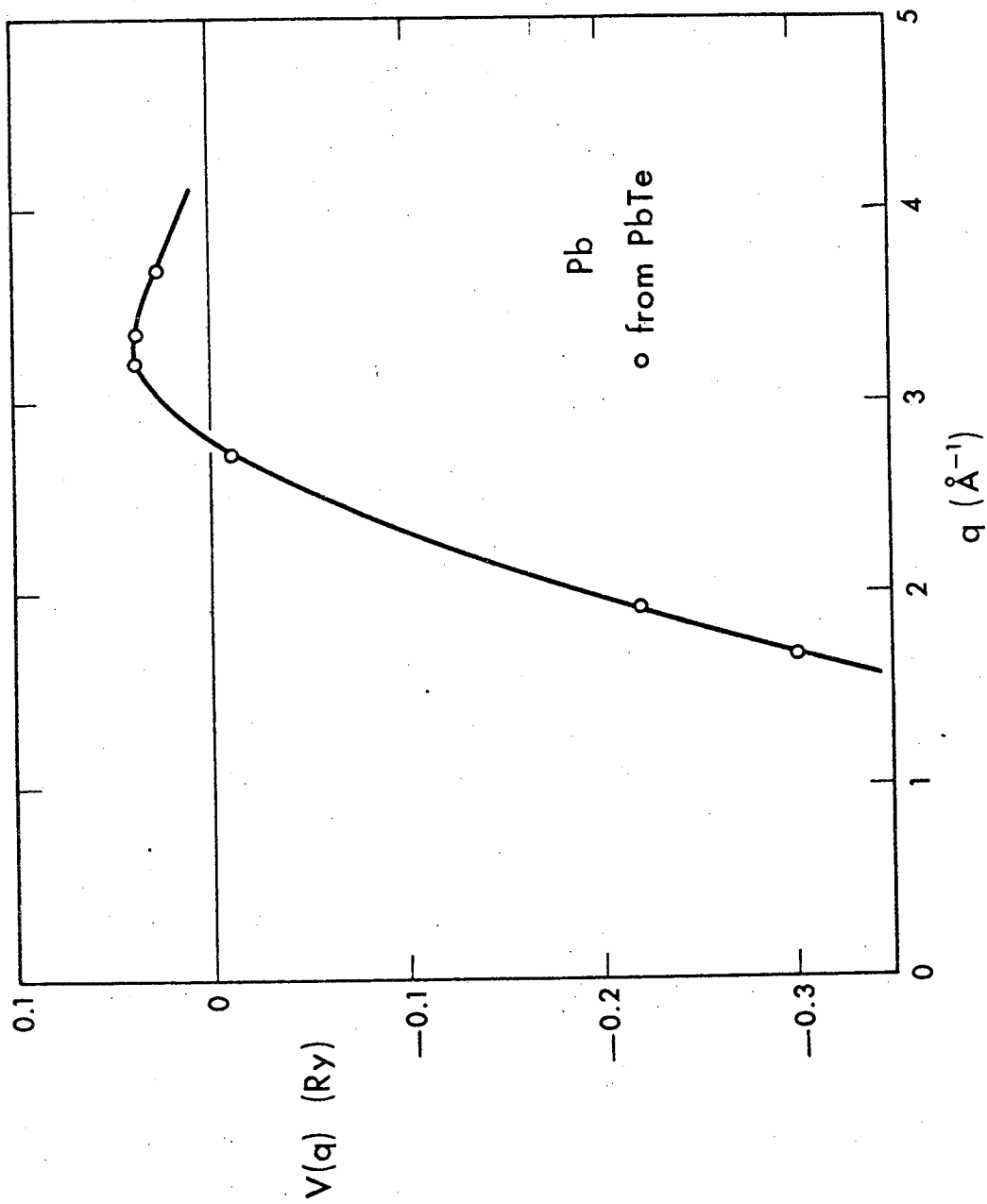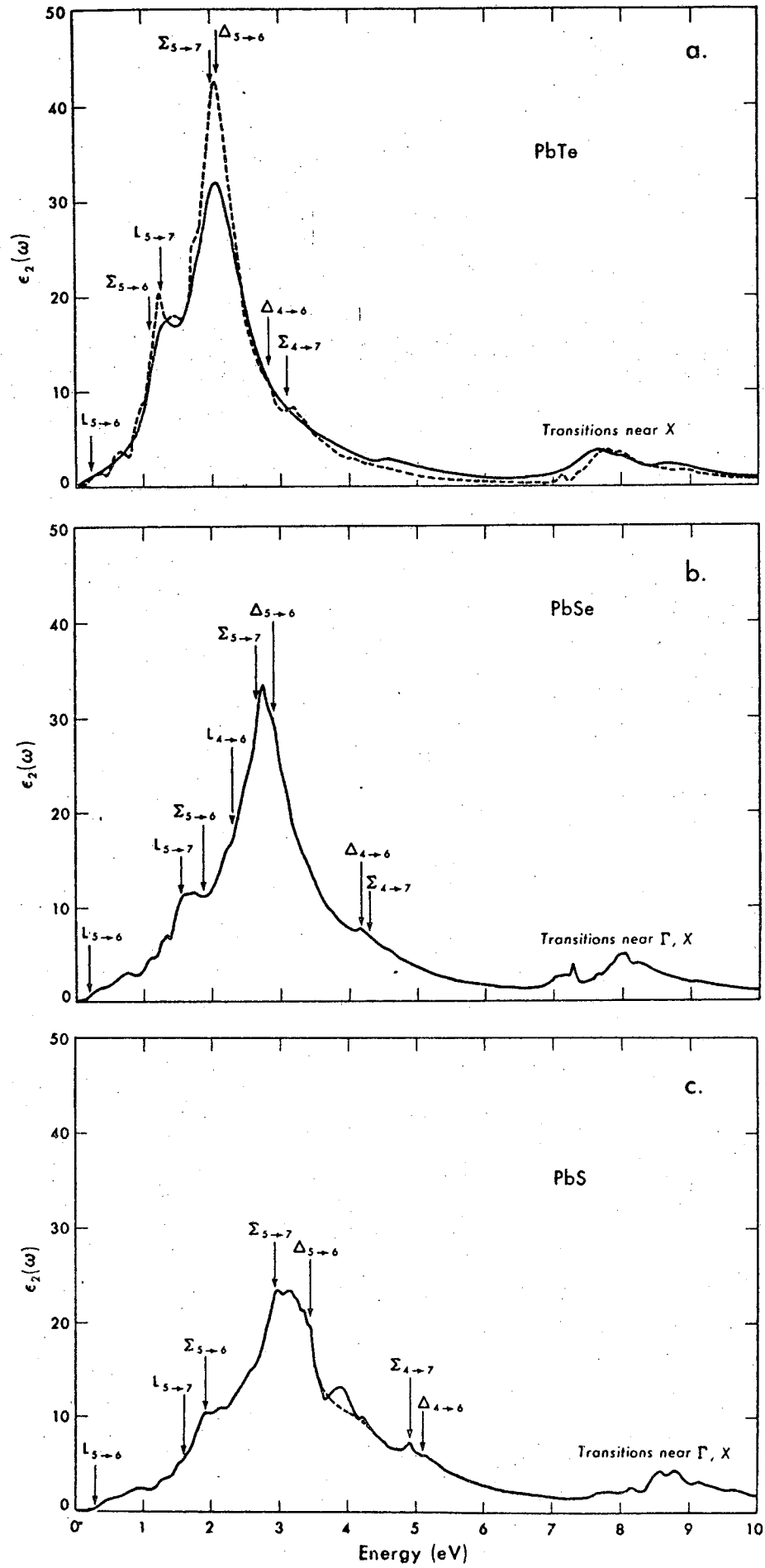
Energy (eV)

Fig. 11

XBL723-6080

Fig. 12

Fig. 13(a)

Density of states

Fig. 13(b)

PbSe

LBL-1132

Fig. 13(c)